*Capillarity*

Vol. 5, No. 3, p. 41-50, 2022

Original article

# Modeling of two-phase flow in heterogeneous wet porous media

Yihang Xiao[1], Yongming He[1]*, Jun Zheng[1], Jiuyu Zhao[2]

[1]*College of Energy, Chengdu University of Technology, Chengdu 610059, P. R. China*

[2]*State Key Laboratory of Petroleum Resources and Prospecting, China University of Petroleum, Beijing 102249, P. R. China*

**Keywords:**
Heterogeneous wet system
two-phase flow
capillary bundle model
capillary pressure
relative permeability

**Cited as:**
Xiao, Y., He, Y., Zheng, J., Zhao, J. Modeling of two-phase flow in heterogeneous wet porous media. Capillarity, 2022, 5(3): 41-50.
https://doi.org/10.46690/capi.2022.03.01

**Abstract:**
The characterization of two-phase flow has been commonly based on homogeneous wet capillary models, which are limited to heterogeneous wet porous media. In this work, capillary pressure and relative permeability models for three heterogeneous wet systems are derived, which enable the analysis of the effect of oil-wet ratio on the two-phase flow mechanism. The capillary pressures, relative permeabilities and water cut curves of three systems are simulated at the primary drainage stage. The results show that water-wet and oil-wet systems exhibit drainage and imbibition characteristics, respectively, while heterogeneous wet systems show both of these characteristics, and a large oil-wet ratio is favourable to oil imbibition. Mixed-wet large and mixed-wet small systems have water-wet and oil-wet characteristics, respectively, at the end and the beginning of oil displacement. At the drainage stage, the oil-wet ratio can significantly decrease oil conductivity, while water conductivity is enhanced. The conductivity difference between oil and water firstly decreases and then increases with rising water saturation, and the difference diminishes with the increase in oil-wet ratio. The oil-wet ratio can reduce water displacement efficiency, and its effects on the water cut curves vary between the three systems due to wettability distribution and pore-size mutation. The mixed-wet small system has the strongest oil imbibition ability caused by the largest capillary pressure in oil-wet pores and the smallest drainage pressure in water-wet pores, and high water conductivity causes the greatest water cut. The trend of variations in the mixed-wet large system is opposite to that in the mixed-wet small system, and the fractional-wet system is located between the other two systems.

## 1. Introduction

Early studies concluded that the wettability of oil reservoirs is homogeneous (water-wet or oil-wet) (Nutting, 1934; Craig, 1971). With the advancement of experimental methods, it was gradually recognized that reservoir wettability is heterogeneous (Alhammadi et al., 2020; Gao et al., 2020; Pierez et al., 2020; Cai, 2021; Elakneswaran et al., 2021). The reservoir conditions can be extremely complex, as numerous uncertain factors provide formation conditions for heterogeneous wet systems, such as mineral species, pore geometry, fluid chemistry, pore surface roughness, fluid-pore surface contact time, interfacial tension, temperature, and pressure (Kjosavik et al., 2002). In addition, a large number of tertiary recovery techniques, such as surfactant displacement, alkali displacement, $CO_2$ displacement, may cause a variation in the original reservoir wettability and make it complex (Chang et al., 2020; Diao et al., 2021; Zheng et al., 2021; Wu et al., 2022).

The heterogeneous wet phenomenon indicates the presence of hydrophilic and oleophilic surfaces, which can increase the complexity of the two-phase flow mechanism. The heterogeneous wetting system is generally divided into two types: 1) a mixed-wetting system where wettability is distributed according to pore size, including mixed-wet large (MWL) (Skauge et

Yandy Scientific Press

*Corresponding author.
*E-mail address*: xiaoyihang@stu.cdut.edu.cn (Y. Xiao); heyongming09@cdut.edu.cn (Y. He); ouyeada@163.com (J. Zheng); 2020310039@student.cup.edu.cn (J. Zhao).



Received April 20, 2022; revised May 19, 2022; accepted May 25, 2022; available online May 28, 2022.

al., 2003) and mixed-wet small (MWS) (Skauge et al., 2007), where large and small pores are oil-wet, respectively; and 2) a fractional wetting (FW) system (Jerauld and Rathmell, 1997) where wettability is uncorrelated to pore size. Numerous experimental studies have shown that the FW system is the most common one for oil reservoirs (Dodd et al., 2014).

Capillary pressure and relative permeability are the intrinsic equations of multi-phase flow (Anderson, 1987; Cai et al., 2014; El-Amin et al., 2017; Jiao et al., 2020), therefore, these have been subjected to experiments with artificial FW systems. Usually, physical models for artificial porous media are packed with quartz sand (water-wet) and polytetrafluoroethylene (PTFE) particles (oil-wet) in different proportions but the same grain size, thus models have a different oil-wet ratio k, which is the ratio of oil-wet particle volume to total particle volume. Thus far, the effect of $k$ on the flow mechanism of the FW system has been comprehensively and uniformly understood (Bauters et al., 2000; Hwang et al., 2006; Falode and Manuel, 2014). However, experimental studies on MWL and MWS systems are challenging because their artificial porous media are not currently possible to manufacture.

Early theoretical studies mainly focused on capillary pressure empirical models for the FW system, and several capillary pressure models have been proposed since. However, the simulation results have poor fitting with experimental data as the empirical parameters lack clear physical meanings, and these models can only be used for prediction in water-wet and oil-wet systems. Ustohal et al. (1998) proposed a phenomenological model with meaningful parameters that can simulate the FW system, while the abundant input parameters limit its application range. O'Carroll et al. (2005) put forward a model with clear physical meaning parameters. However, purely positive or negative capillary pressure curves could still not be simulated.

As an alternative approach, the formation mechanism of heterogeneous wet systems was applied to pore-scale modeling (Kovscek et al., 1993). However, the two-phase flow and variation equations are complex and difficult to calculate in a real 3D (three-dimensional) pore network model (Nemer et al., 2020). To simplify the pore network, a capillary bundle model or a 3D ideal model was used. Several studies applied the thin-film theory to the capillary bundle model and the 3D network model with equilateral triangular cross-sectional pores, and subsequent capillary pressure or relative permeability models were proposed by the work-energy conversion theory (Hui and Blunt, 2000; Helland and Skjaeveland, 2004; Valvatne and Blunt, 2004). Unfortunately, the above models can only simulate the flow rules of the MWL system due to the single pore shape and the simplified mechanism of wettability change. Therefore, Kallel et al. (2017) improved the wettability variation criterion proposed by Blunt (1997) by using combinations of different pore shapes, to simulate two-phase flows of the MWS and FW systems. Zhao et al. (2018) simulated the effect of k on the relative permeability curves based on the Lattice Boltzmann model and derived the 2D fluid distribution for separate displacement stages. Zheng et al. (2021) proposed the fluid distribution and displacement process of cylindrical FW capillary, and studied the effect of $k$ on capillary pressure curves.

However, a unified two-phase flow model has been challenging to obtain owing to the complex combination of pore shapes and the actual reservoir wettability change mechanism (Kovscek et al., 1993). In this work, we investigate the two-phase flow in heterogeneous wet systems, which provides significant aid to simplify the above problem. Moreover, the cylindrical capillary bundle is adopted as the pore structure to establish different wettability distributions, and the capillary pressure and relative permeability models of three heterogeneous wet systems are derived based on the flow equations (Young-Laplace equation and conductivity equation). Subsequently, the two-phase flows of MWL, MWS and FW systems are simulated, and the differences between them are analyzed.

## 2. Model descriptions

### 2.1 Fundamental equations

The "3R modeling method" suggests that, although the exact characteristics of the real pore are unknown, three important parameters (pore volume $V(r)$, conductivity $g_c$ and capillary pressure $P_c$) can be obtained from the pore radius. A cylindrical capillary for the pore structure and homogeneous wetting for the pore surface are assumed (oil-wet or water-wet). The capillary pressure can be expressed by the Young-Laplace equation:

$$P_c = \frac{2\sigma\cos\theta}{r} \tag{1}$$

where $r$ denotes cross-sectional radius, $\sigma$ denotes interfacial tension, and $\theta$ is the contact angle.

When the oil enters the water-wet pores ($\theta < 90°$), the capillary pressure acts as a force of resistance. A larger $r$ leads to a smaller $P_c$, whereby this benefits oil displacement. This rule is the opposite when the oil enters the oil-wet pores ($\theta > 90°$).

The one-phase conductivity in the cylindrical capillary follows Fourier's law (Purcell, 1949), such as:

$$g_c = \frac{\pi r^4}{8\mu} \tag{2}$$

where $\mu$ denotes fluid viscosity.

### 2.2 Pore size distribution and capillary bundle model

The pore size distribution is described by the lognormal distribution function, and we consider that it is adequate to characterize a wide range of core samples (Kosugi, 1994). The density function $f(r)$ is then given by the formula:

$$f(r) = \frac{1}{\sqrt{2\pi}\lambda r}\exp\left[-\frac{(\ln r-\eta)^2}{2\lambda^2}\right], \; r_{\min} \le r \le r_{\max} \tag{3}$$

where $\eta$ denotes the mean, $\lambda$ denotes the variance; $r_{\min}$ and $r_{\max}$ are the minimum and maximum capillary radius, respectively; their values in this paper are $\eta = 1.14$, $\lambda = 0.58$, $r_{\min} = 0.01$ $\mu$m, and $r_{\max} = 20$ $\mu$m.

The pore volume $V_p$ of the capillary bundle model is expressed as:

$$V_p = \int_{r_{\min}}^{r_{\max}} f(r)V(r)dr \tag{4}$$

The water saturation $S_w$ of the capillary bundle model can be expressed as:

$$S_w = \frac{V_w}{V_p} \tag{5}$$

where $V_w$ denotes water volume in the capillary bundle model.

Assuming that the capillary bundle model is initially saturated with water. For water-wet pores, when the displacement pressure reaches the capillary entry pressure $P_{cw}^e$, oil enters the capillary bundle by piston-like drainage, the corresponding $r$ is the minimum critical radius $r_{cw}$, and $P_{cw}^e > 0$. For oil-wet pores, when the displacement pressure reaches the capillary entry pressure $P_{co}^e$, oil enters the capillary bundle by piston-like imbibition, the corresponding $r$ takes the value of maximum critical radius $r_{co}$, and $P_{co}^e < 0$. Two capillary entry pressures can be expressed as:

$$P_{cw}^e = \frac{2\sigma \cos\theta}{r_{cw}} \tag{6a}$$

$$P_{co}^e = \frac{2\sigma \cos\theta}{r_{co}} \tag{6b}$$

The one-phase conductivity $g_s$ in the cylindrical capillary bundle model is:

$$g_s = \int_{r_{\min}}^{r_{\max}} f(r)g_c(r)dr \tag{7}$$

For the capillary bundle model, absolute permeability is a constant and is proportional to the conductivity. Thus, the relative permeability of water and oil ($K_{rw}$, $K_{ro}$) can be calculated by:

$$K_{rw} = \frac{g_w}{g_s} \tag{8a}$$

$$K_{ro} = \frac{g_o}{g_s} \tag{8b}$$

where $g_w$ and $g_o$ respectively represent water and oil conductivity.

According to the wettability distribution of different heterogeneous wet systems, the capillary pressure and relative permeability models can be derived by combining the displacement pressure, the corresponding $S_w$, $K_{rw}$ and $K_{ro}$.

## 2.3 Wettability distribution

For the MWL system, pores larger than the wettability critical radius $r_m$ are oil-wet and those smaller than $r_m$ are water-wet (Fig. 1(a)); the opposite is true for the MWS system (Fig. 1(b)). In the FW system, oil-wet and water-wet pores coexist in all pore size distributions, and $k$ is constant (Fig. 1(c)).

The relationships between $r_m$ and $k$ for the MWL and MWS systems are established as:

$$k_{MWL} = \frac{\int_{r_m}^{r_{\max}} f(r)V(r)dr}{\int_{r_{\min}}^{r_{\max}} f(r)V(r)dr} \tag{9a}$$

$$k_{MWS} = \frac{\int_{r_{\min}}^{r_m} f(r)V(r)dr}{\int_{r_{\min}}^{r_{\max}} f(r)V(r)dr} \tag{9b}$$

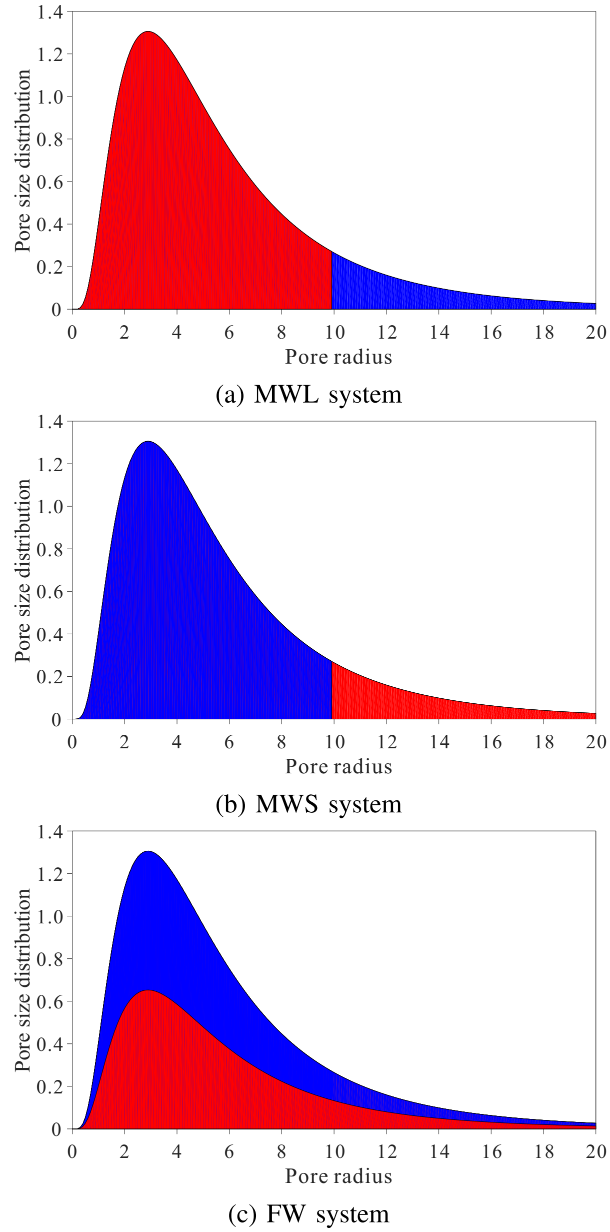


**Fig. 1**. Wettability distributions of heterogeneous wet systems when $k = 1/2$ (the red area indicates oil-wet pores, and the blue area indicates water-wet pores).

With the increase in $r_m$, the $k_{MWL}$ decreases, while this is the opposite for $k_{MWS}$.

For the FW system, assuming that the oil-wet pore size distribution function is $f_o(r)$, the water-wet pore size distribution function is $f_w(r)$, and $f_o(r) + f_w(r) = f(r)$. Then, the $k_{FW}$ can be expressed by:

$$k_{FW} = \frac{\int_{r_{\min}}^{r_{\max}} f_o(r)V(r)dr}{\int_{r_{\min}}^{r_{\max}} f(r)V(r)dr} \tag{10}$$

## 2.4 Capillary pressure and relative permeability models

Heterogeneous wet systems consist of oil-wet pores ($\theta_o = 170°$) and water-wet pores ($\theta_w = 10°$), and the oil-water interfacial tension $\sigma_{ow} = 0.26$ N/m. The $k$ values are 0, 1/4, 1/2, 3/4, and 1, where $k = 0$ and $k = 1$ indicate the water-wet and oil-wet systems, respectively. The capillary bundle model is initially saturated with water, and the oil enters the capillary bundle by the $P_c$ transited from negative infinity to positive infinity.

When oil imbibition into the oil-wet pores occurs ($P_c < 0$) $S_w$ for MWL, MWS, and FW systems can be respectively calculated by:

$$S_{w,MWL} = \frac{\int_{r_{\min}}^{r_m} f(r)V(r)dr + \int_{r_{co}}^{r_{\max}} f(r)V(r)dr}{\int_{r_{\min}}^{r_{\max}} f(r)V(r)dr} \tag{11a}$$

$$S_{w,MWS} = \frac{\int_{r_m}^{r_{\max}} f(r)V(r)dr + \int_{r_{co}}^{r_m} f(r)V(r)dr}{\int_{r_{\min}}^{r_{\max}} f(r)V(r)dr} \tag{11b}$$

$$S_{w,FW} = \frac{\int_{r_{co}}^{r_{\max}} f_o(r)V(r)dr + \int_{r_{\min}}^{r_{\max}} f_w(r)V(r)dr}{\int_{r_{\min}}^{r_{\max}} f(r)V(r)dr} \tag{11c}$$

The values of $K_{rw}$ and $K_{ro}$ for the oil imbibition stage for MWL, MWS, and FW systems can be respectively calculated by:

$$K_{rw,MWL} = \frac{\int_{r_{\min}}^{r_m} f(r)g_c(r)dr + \int_{r_{co}}^{r_{\max}} f(r)g_c(r)dr}{\int_{r_{\min}}^{r_{\max}} f(r)g_c(r)dr} \tag{12a}$$

$$K_{ro,MWL} = \frac{\int_{r_m}^{r_{co}} f(r)g_c(r)dr}{\int_{r_{\min}}^{r_{\max}} f(r)g_c(r)dr} \tag{12b}$$

$$K_{rw,MWS} = \frac{\int_{r_m}^{r_{\max}} f(r)g_c(r)dr + \int_{r_{co}}^{r_m} f(r)g_c(r)dr}{\int_{r_{\min}}^{r_{\max}} f(r)g_c(r)dr} \tag{13a}$$

$$K_{ro,MWS} = \frac{\int_{r_{\min}}^{r_{co}} f(r)g_c(r)dr}{\int_{r_{\min}}^{r_{\max}} f(r)g_c(r)dr} \tag{13b}$$

$$K_{rw,FW} = \frac{\int_{r_{co}}^{r_{\max}} f_o(r)g_c(r)dr + \int_{r_{\min}}^{r_{\max}} f_w(r)g_c(r)dr}{\int_{r_{\min}}^{r_{\max}} f(r)g_c(r)dr} \tag{14a}$$

$$K_{ro,FW} = \frac{\int_{r_{\min}}^{r_{co}} f_o(r)g_c(r)dr}{\int_{r_{\min}}^{r_{\max}} f(r)g_c(r)dr} \tag{14b}$$

Once the oil has saturated all oil-wet pores, when the oil enters the water-wet pores ($P_c > 0$), the $S_w$ for MWL, MWS, and FW systems can be respectively calculated by:

$$S_{w,MWL} = \frac{\int_{r_{\min}}^{r_{cw}} f(r)V(r)dr}{\int_{r_{\min}}^{r_{\max}} f(r)V(r)dr} \tag{15a}$$

$$S_{w,MWS} = \frac{\int_{r_m}^{r_{cw}} f(r)V(r)dr}{\int_{r_{\min}}^{r_{\max}} f(r)V(r)dr} \tag{15b}$$

$$S_{w,FW} = \frac{\int_{r_{\min}}^{r_{cw}} f_w(r)V(r)dr}{\int_{r_{\min}}^{r_{\max}} f(r)V(r)dr} \tag{15c}$$

The values of $K_{rw}$ and $K_{ro}$ for the oil drainage stage for MWL, MWS, and FW systems can be respectively calculated by:

$$K_{rw,MWL} = \frac{\int_{r_{\min}}^{r_{cw}} f(r)g_c(r)dr}{\int_{r_{\min}}^{r_{\max}} f(r)g_c(r)dr} \tag{16a}$$

$$K_{ro,MWL} = \frac{\int_{r_m}^{r_{\max}} f(r)g_c(r)dr + \int_{r_{cw}}^{r_{\min}} f(r)g_c(r)dr}{\int_{r_{\min}}^{r_{\max}} f(r)g_c(r)dr} \tag{16b}$$

$$K_{rw,MWS} = \frac{\int_{r_m}^{r_{cw}} f(r)g_c(r)dr}{\int_{r_{\min}}^{r_{\max}} f(r)g_c(r)dr} \tag{17a}$$

$$K_{ro,MWS} = \frac{\int_{r_{cw}}^{r_{\max}} f(r)g_c(r)dr + \int_{r_{\min}}^{r_m} f(r)g_c(r)dr}{\int_{r_{\min}}^{r_{\max}} f(r)g_c(r)dr} \tag{17b}$$

$$K_{rw,FW} = \frac{\int_{r_{\min}}^{r_{cw}} f_w(r)g_c(r)dr}{\int_{r_{\min}}^{r_{\max}} f(r)g_c(r)dr} \tag{18a}$$

$$K_{ro,FW} = \frac{\int_{r_{\min}}^{r_{\max}} f_o(r)g_c(r)dr + \int_{r_{cw}}^{r_{\max}} f_w(r)g_c(r)dr}{\int_{r_{\min}}^{r_{\max}} f(r)g_c(r)dr} \tag{18b}$$

## 3. Results and discussion

### 3.1 Capillary pressure curves

Fig. 2 shows the capillary pressure curves of the three heterogeneous wet systems, which reveal the imbibition ability of the wetting phase in porous media. The top blue and bottom red curves of the group, which correspond to the drainage and imbibition processes of the conventional water-wet ($k = 0$) and oil-wet ($k = 1$) systems, respectively, are centrosymmetric. However, other curves with $k$ values are located between them, following the trend that the capillary pressures gradually move downward with the increase in $k$, and feature both drainage and imbibition processes.

For the MWL and MWS systems, the curves with different $k$ values overlap with the water-wet and oil-wet systems, respectively. The water saturation range of overlap decreases and increases, respectively, with the increase in $k$ in the MWL and MWS systems. The number of oil-wet pores increases with the growth of $k$, thus oil enters water-wet pores (where the inflection point occurs) at lower $S_w$ for the MWL and MWS systems. There is no overlapping phenomenon (without any inflection points) for the FW system caused by the difference in wettability distribution, and the curves are close to oil-wet and water-wet systems at high and low $S_w$, respectively.

Wettability distribution is the main reason for the difference in two-phase flow rules. In the imbibition stage, oil firstly enters the oil-wet pores of the minimum radius, and the imbibition process is stopped when oil as the non-wetting phase enters water-wet pores of the maximum radius. When water-wet pores of the minimum radius are saturated, the whole displacement process is completed. For the MWS and MWL systems, the radius and contact angle of the maximum-radius oil-wet pore and water-wet pore are largely different (these are respectively called pore-size mutation and contact angle hysteresis), thus the water phase needs higher pressure to enter the water-wet pore, resulting in a discontinuous curve. However, for the FW system, the maximum radii of the oil-wet pore space and water-wet pore space are equal, and only the wetting hysteresis exists, resulting in a minimal discontinuity in the curve.

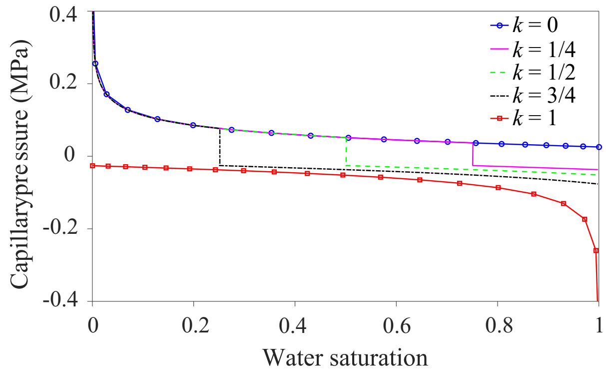


(a) MWL system

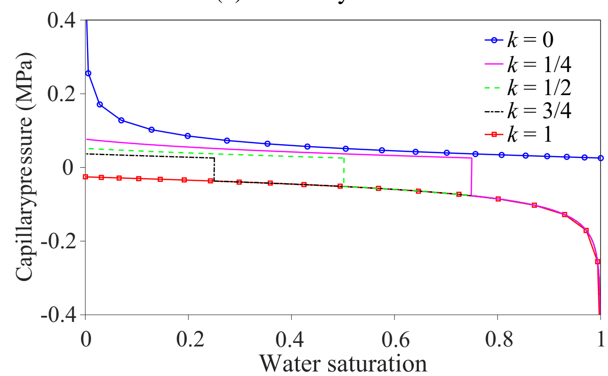


(b) MWS system

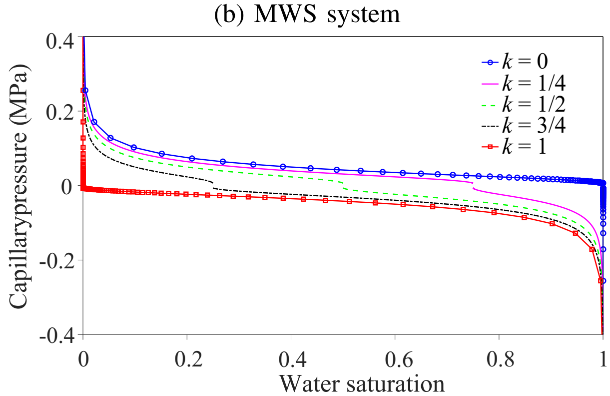


(c) FW system

**Fig. 2**. Capillary pressure curves of different heterogeneous wet systems.

## 3.2 Relative permeability curves

Fig. 3 shows the relative permeability curves and relative permeability ratio curves of different systems. The relative permeability curves of uniform wetting systems are symmetrically distributed around $S_w = 0.5$, and other curves with $k$ are located between them. $K_{ro}$ decreases and $K_{rw}$ increases for the same $S_w$ with the increase in $k$, and the point of $K_{ro} = K_{rw}$ moves to lower $S_w$ to achieve higher oil conductivity. For the MWL system, a higher $k$ indicates the decrease in $r_m$, which leads to weakened oil conductivity, while water can enter larger oil-wet pores at lower $S_w$ when water has saturated all water-wet pores, which in turn enhances the water flowing ability. For the MWS system, the $r_m$ rises with the increase in $k$, thus water also can enter larger oil-wet pores at lower $S_w$, which is opposite to the MWL system. For the FW system, oil can occupy smaller pores with the increase in $k$, which reduces oil flowability, while this situation enhances water flowability. According to the above analysis, the flow mechanisms of the three heterogeneous wet systems are significantly different.

The relative permeability curves of the MWL and MWS systems overlap with the water-wet and oil-wet systems, respectively, which is the same for the capillary pressure curves (Fig. 2); the explanations can be found in Subsection 3.1. Meanwhile, the curves of MWL and MWS systems both show obvious inflection points due to the pore-size mutation and contact angle hysteresis.

The relative permeability ratio curve can characterize the difference in two-phase conductivity between different flow stages. A value close to 1 means a smaller conductivity difference. The curves of water-wet and oil-wet systems are parallel to each other in semi-logarithmic coordinates, and the other curves are located between them. The conductivity difference first decreases and then rises with the increase in $S_w$, and the curves gradually move upward with the increase in $k$. At the beginning of the water displacement process, water enters the maximum oil-wet pores at lower $S_w$ with increasing $k$, resulting in the conductivity of water gradually approaching that of oil. As the water displacement process continues, the conductivity difference gradually increases such that the water dominates the flow process at a lower $S_w (K_{rw}/K_{ro} > 1)$, especially in systems with high $k$ value.

## 3.3 Water cut curves

The water cut curve can reflect the water displacement efficiency under various stages. Fig. 4 depicts the water cut curves of different systems. the water cut is less than 0.02 represents the water-free cut stage; the water cut is $0.02 \sim 0.2$ represents the low water cut stage; the water cut is $0.2 \sim 0.6$ represents the medium water cut stage; the water cut is $0.6 \sim 0.9$ represents the high water cut stage; the water cut is $0.9 \sim 0.98$ represents the ultra-high water cut stage. The water cut curves with the change of $k$ are located between the uniform wetting systems, and the water cut is positively related to $k$ for the same $S_w$, which means that the water displacement efficiency becomes worse with the increase in $k$. For the MWL system, the water cut curve shows a trend of slowly and then rapidly increasing with the rise of $S_w$, and the change magnitude increases with the decrease in $k$. This phenomenon is caused by two reasons: one is that water firstly enters water-wet small pores; this changing trend of water cut is a gradual effect of the relatively small pore volume (Fig. 1(a)). Then, water enters the largest oil-wet pores at the inflection point (corresponding $k$) of the curve, and the larger oil-wet pore volume can lead to an obvious increase in water cut. The other reason is that water enters oil-wet pores at a larger pore radius with the increase in $k$, resulting in the rising trend of water cut being more dramatic. For the MWS system, the water cut increases rapidly and then slowly, and the change magnitude increases with the enhancement of $k$; the percolation mechanism is the opposite for the MWL system. For the FW system, the curve trend is relatively flat at low

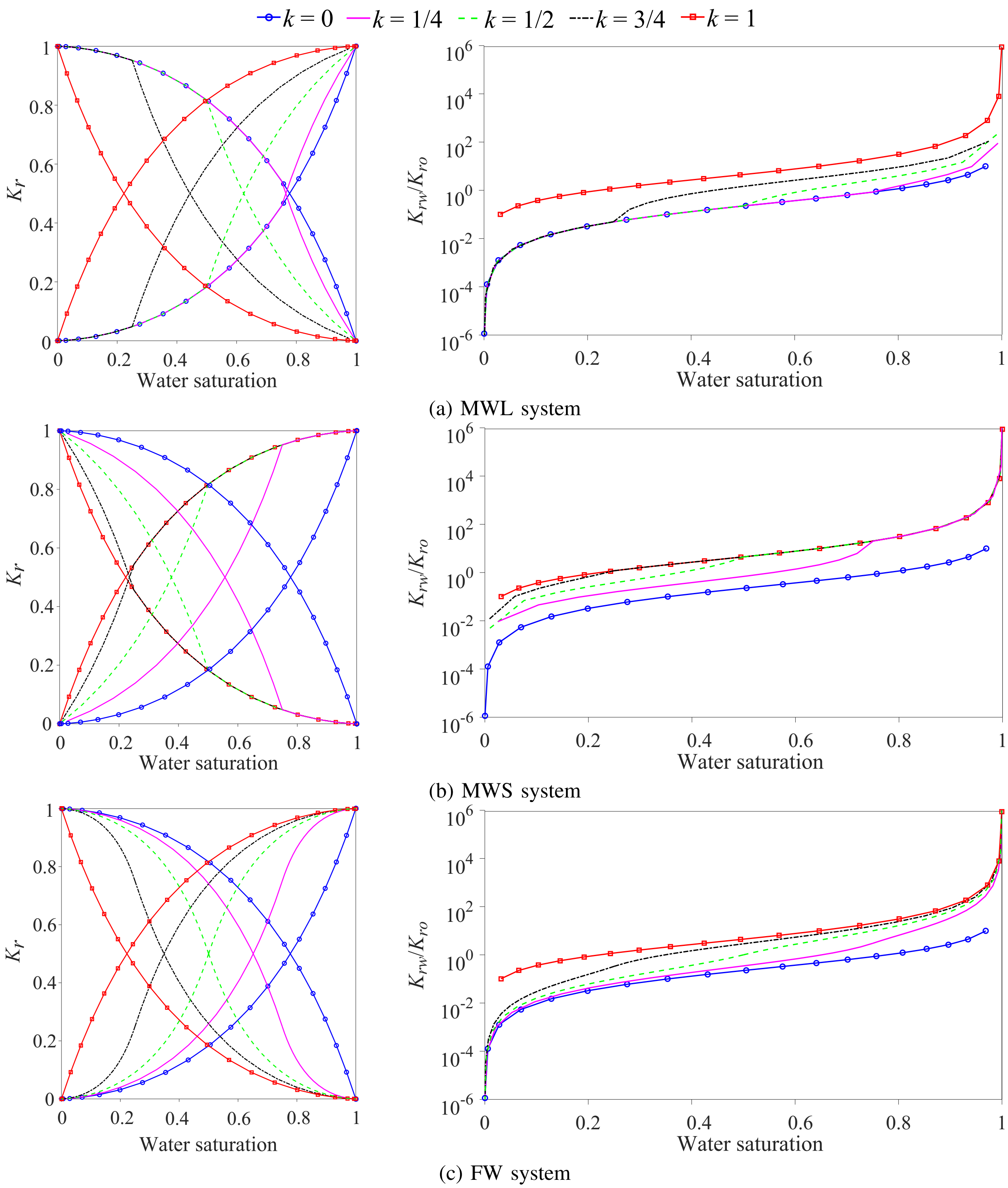


**Fig. 3**. Relative permeability curves and relative permeability ratio curves of heterogeneous wet systems.

and high $S_w$ values due to the fact that there is no pore-size mutation.

### *3.4 Comparison of heterogeneous wet systems*

Based on the capillary pressure curves of the three heterogeneous wet systems (Fig. 5), the curve of the FW system is symmetrical to $S_w = 0.5$ when $k = 1/2$, and the curves of the MWL and MWS systems are symmetrically distributed around the FW system. For the MWS system, the oil imbibition ability is the strongest in the imbibition stage owing to the greatest capillary pressure; in the drainage stage, oil can enter the water-wet pores at lower capillary pressure, resulting in the curves of the MWS system located below those of the MWL system. The curve of the FW system is between the other two systems.

As can be seen from the relative permeability curves (Fig. 6), the oil relative permeability curve of the MWL system is shifted to the right, which indicates that the oil phase is more

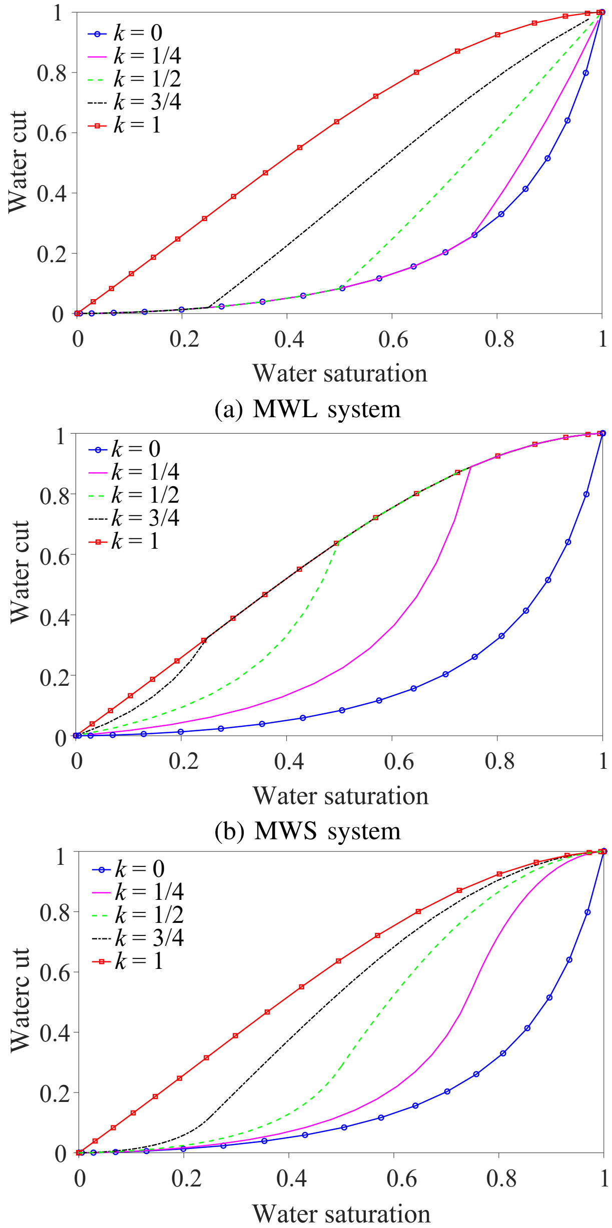


**Fig. 4**. Water cut curves of heterogeneous wet systems.

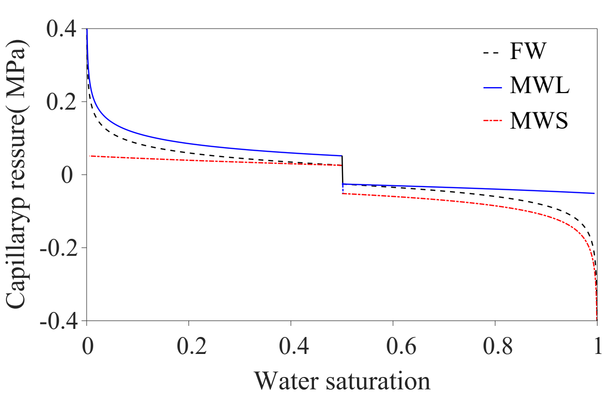


**Fig. 5**. Capillary pressure curves of heterogeneous wet systems ($k = 1/2$).

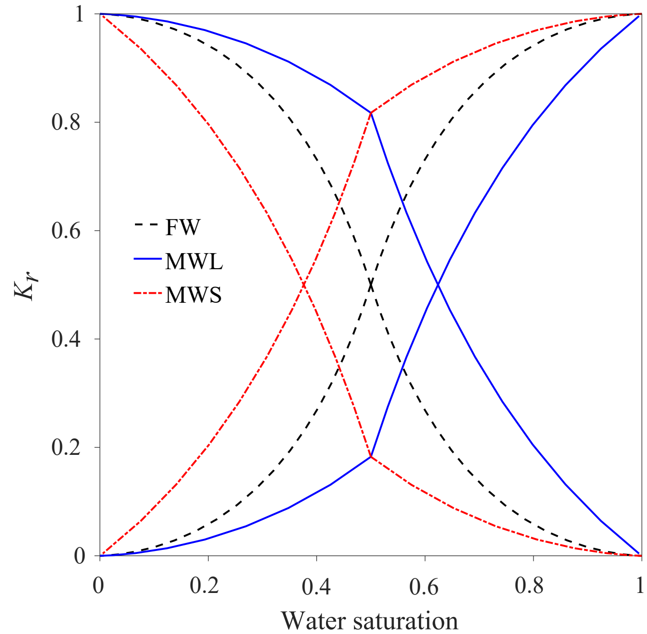


**Fig. 6**. Relative permeability curves of heterogeneous wet systems ($k = 1/2$).

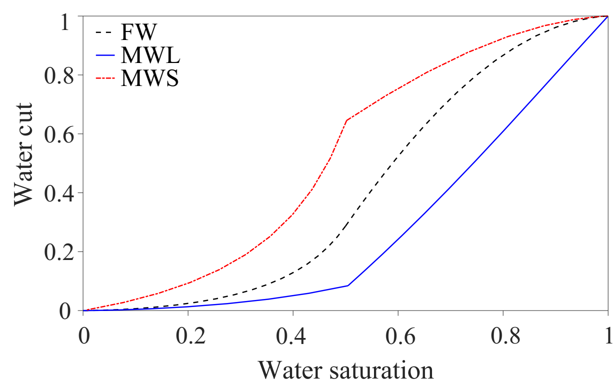


**Fig. 7**. Water cut curves of heterogeneous wet systems ($k = 1/2$).

likely to occupy large pores under the same $S_w$. $K_{rw}$ is the largest under the same $S_w$ for the MWS system, which is caused by water mainly occupying large pores. The curve of the FW system is between the other two and symmetrically distributed to $S_w = 0.5$. For the water cut curves (Fig. 7), the MWS system with the highest water content leads to the poorest water displacement efficiency, the MWL system has a great water displacement efficiency, and the FW system is between the other two systems.

### 3.5 Discussion and comparison of previous models

Bradford and Leij (1996) put forward a capillary pressure model of the FW system:

$$P_c^{FW}(S_w) = P_c^{ww}(S_w) - \alpha \tag{19}$$

where $P_c^{FW}$ and $P_c^{ww}$ represent the capillary pressure of FW system and water-wet system, respectively, and $\alpha$ is a constant that is related to the oil-wet ratio. However, this model cannot simulate the capillary pressure curve of the oil-wet system by shifting $\alpha$.

Skjaeveland et al. (2000) treated the positive and negative portions of curves as an individual model and proposed a capillary pressure model of the FW system, such as:

$$P_c^{FW}(S_w) = c_w P_c^{ww}(S_w) + c_o P_c^{ow}(S_o) \tag{20}$$

where $P_c^{ow}$ denotes the capillary pressure of oil-wet system; $c_w$ and $c_o$ are constants, and $c_w = 1$, $c_o = 0$ and $c_w = 0$, $c_o = 1$ for the water-wet and oil-wet system, respectively. However, $c_w$ and $c_o$ are difficult to select for the FW system.

O'Carroll et al. (2005) presented a capillary pressure model of the FW system based on Leverett's scaling function and the Cassie-Baxter function, which (without empirical constants) is expressed as:

$$P_c^{FW}(S_w) = (1-k)\cos\theta_w P_c^{ww}(S_w) + k\cos\theta_o P_c^{ow}(S_o) \tag{21}$$

where $S_o$ denotes oil saturation. However, this model lacks a definite physical meaning of the Cassie-Baxter function (Cassie and Baxter, 1944) for the FW system.

Therefore, the aforementioned empirical models cannot accurately simulate the capillary pressure of the FW system, and no empirical models exist for the MWL and MWS systems. Currently, the pore-scale models of capillary pressure and relative permeability are established by polygonal pore and MS-P theory (Mayer and Stowe, 1965; Princen, 1969a, 1969b; Princen, 1970). However, the solution of these models is very difficult to obtain due to the complex formation process of pores and the combination of pore shapes. The models proposed in this work can well simulate two-phase flows for three heterogeneous wet systems, and the simulation accuracy and applicability are superior to existing empirical models. However, certain disadvantages of the model in this paper are also inevitable. For example, there are no irreducible phases, as the pore connectivity is not considered. Moreover, the capillary pressure curves and relative permeability curves have inflection points due to pore-size mutation and contact angle hysteresis, although the FW system is an exception owing to the existence of contact angle hysteresis. Compared to fine pore-scale models, the proposed model is sufficient to describe the processes on a large scale but is not precise on the pore-scale. Therefore, pore-scale heterogeneous wet models based on circular capillary should be further investigated to improve the model of this paper.

## 4. Conclusions

In this work, capillary pressure and relative permeability models were derived for heterogeneous wet systems, to comprehensively study the effect of oil-wet ratio on two-phase flow and the difference between three heterogeneous wet systems. From the proposed models and subsequent computational results, the following conclusions can be drawn:

1) The conventional water-wet ($k = 0$) and oil-wet ($k = 1$) systems only have drainage and imbibition processes, respectively, while heterogeneous wet systems possess both characteristics. The imbibition ability enhances with the increase in oil-wet ratio. For heterogeneous wet systems, there is a start-up pressure in the imbibition process, which is explained by the obvious contact angle hysteresis and pore-size mutation.
2) The MWL and MWS systems have two-phase flow characteristics of water-wet and oil-wet system, respectively, at the end and beginning of oil drainage. However, this phenomenon does not appear in the FW system due to different wettability distributions. A large $k$ value can increase $K_{rw}$ and decrease $K_{ro}$ for the same $S_w$, and the points of $K_{ro} = K_{rw}$ move to the lower $S_w$ to achieve higher oil conductivity.
3) At the beginning of water displacement, water enters the maximum oil-wet pores at lower $S_w$ along with the increase in $k$, resulting in the conductivity of water gradually approaching that of oil. With the water saturation increasing, the conductivity difference gradually increases as the water dominates the flow process, especially in systems with high $k$ value. The water displacement efficiency decreases with the increase in $k$.
4) The MWS system has the strongest oil imbibition ability, which is caused by the largest capillary pressure in the oil-wet pore and the smallest drainage pressure in the water-wet pore. The high water conductivity results in the lowest water displacement efficiency in the MWS system. However, the variation in the MWL system follows the opposite trend. The characterization results for the two-phase flow in the FW system are between those for the MWS and MWL systems.

## Acknowledgement

This work was supported by the National Natural Science Foundation of China (No. 51774053), the Fundamental Research Funds for the Central Universities (No. 2462019YJRC011).

## Conflict of interest

The authors declare no competing interest.



## References

Alhammadi, A. M., Gao, Y., Akai, T., et al. Pore-scale X-ray imaging with measurement of relative permeability, capillary pressure and oil recovery in a mixed-wet microporous carbonate reservoir rock. Fuel, 2020, 268(15): 117018.

Anderson, W. G. Wettability literature survey-Part 4: Effects of wettability on capillary pressure. Journal of Petroleum Technology, 1987, 39(10): 1283-1300.

Bauters, T. W. J., Steenhuis, T. S., Dicarlo, D. A., et al. Physics of water repellent soils. Journal of Hydrology, 2000, 231-232(29): 233-243.

Blunt, M. J. Pore level modeling of the effects of wettability. SPE Journal, 1997, 2(4): 494-510.

Bradford, S. A., Leij, F. J. Predicting two- and three-fluid capillary pressure saturation relationships of porous media with fractional wettability. Water Resources Research, 1996, 32(2): 251-259.

Cai, J. Some key issues and thoughts on spontaneous imbibition in porous media. Chinese Journal of Computational Physics, 2021, 38(5): 505-512. (in Chinese)

Cai, J., Perfect, E., Cheng, C. L., et al. Generalized modeling of spontaneous imbibition based on Hagen-Poiseuille flow in tortuous capillaries with variably shaped apertures. Langmuir, 2014, 30(18): 5142-5151.

Cassie, A. B. D., Baxter, S. Wettability of porous surfaces. Transactions of the Faraday Society, 1944, 40(1): 546-551.

Chang, C., Kneafsey, T. J., Wan, J., et al. Impacts of mixed-wettability on brine drainage and supercritical $CO_2$ storage efficiency in a 2.5-D heterogeneous micromodel. Water Resources Research, 2020, 56(7): e2019WR026789.

Craig, F. F. The Reservoir engineering aspects of waterflooding. SPE Monograph Series, 1971.

Diao, Z., Li, S., Liu, W., et al. Numerical study of the effect of tortuosity and mixed wettability on spontaneous imbibition in heterogeneous porous media. Capillarity, 2021, 4(3): 50-62.

Dodd, N., Marathe, R., Middleton, J., et al. Pore-scale imaging of oil and wettability in native-state, mixed-wet reservoir carbonates. Paper SPE 17696 Presented at International Petroleum Technology Conference, Doha, Qatar, 19-22 January, 2014.

Elakneswaran, Y., Ubaidah, A., Takeya, M., et al. Effect of electrokinetics and thermodynamic equilibrium on low-salinity water flooding for enhanced oil recovery in sandstone reservoirs. ACS Omega, 2021, 6(5): 3727-3735.

El-Amin, M., Kou, J., Sun, S., et al. Adaptive time-splitting scheme for two-phase flow in heterogeneous porous media. Advances in Geo-Energy Research, 2017, 1(3): 182-189.

Falode, O., Manuel, E. Wettability effects on capillary pressure, relative permeability, and irredcucible saturation using porous plate. Journal of Petroleum Engineering, 2014, 2014: 465418.

Gao, Y., Raeini, A. Q., Selem, A. M., et al. Pore-scale imaging with measurement of relative permeability and capillary pressure on the same reservoir sandstone sample under water-wet and mixed-wet conditions. Advances in Water Resources, 2020, 146: 103786.

Helland, J. O., Skjaeveland, S. M. Physically based capillary pressure correlation for mixed-wet reservoirs from a bundle-of-tubes model. SPE Journal, 2004, 11(2): 171-180.

Hui, M. H., Blunt, M. J. Effects of wettability on three-phase flow in porous media. Journal of Physical Chemistry B, 2000, 104(16): 3833-3845.

Hwang, S. I., Lee, K. P., Lee, D. S., et al. Effects of fractional wettability on capillary pressure-saturation-relative permeability relations of two-fluid systems. Advances in Water Resources, 2006, 29(2): 212-226.

Jerauld, G. R., Rathmell, J. J. Wettability and relative permeability of prudhoe bay: A case study in mixed-wet reservoirs. SPE Reservoir Engineering, 1997, 12(1): 58-65.

Jiao, L., Andersen, P. Ø., Zhou, J., et al. Applications of mercury intrusion capillary pressure for pore structures: A review. Capillarity, 2020, 3(4): 62-74

Kallel, W., van Dijke, M. I. J., Sorbie, K. S., et al. Pore-scale modeling of wettability alteration during primary drainage. Water Resources Research, 2017, 53(3): 1891-1907.

Kjosavik, A., Ringen, J. K., Skjaeveland, S. M. Relative permeability correlation for mixed-wet reservoirs. SPE Journal, 2002, 7(1): 49-58.

Kosugi, K. Three-parameter lognormal distribution model for soil water retention. Water Resources Research, 1994, 30(4): 891-901.

Kovscek, A. R., Wong, H., Radke, C. J. A pore-level scenario for the development of mixed-wettability in oil reservoirs. Environmental and Energy Engineering, 1993, 39(6): 1072-1085.

Mayer, R. P., Stowe, R. A. Mercury porosimetry-breakthrough pressure for penetration between packed spheres. Journal of Colloid Science, 1965, 20(8): 893-911.

Nemer, M. N., Rao, P. R., Schaefer, L. Wettability alteration implications on pore-scale multiphase flow in porous media using the lattice Boltzmann method. Advances in Water Resources, 2020, 146: 103790.

Nutting, P. G. Some physical and chemical properties of reservoir rocks bearing on the accumulation and discharge of oil. Index of North American Geology, 1934, 12: 825-832.

O'Carroll, D. M., Abriola, L. M., Polityka, C. A., et al. Prediction of two-phase capillary pressure-saturation relationships in fractional wettability systems. Journal of Contaminant Hydrology, 2005, 77(4): 247-270.

Pierez, I., Puntervold, T., Strand, S., et al. Core wettability reproduction: A new solvent cleaning and core restoration strategy for chalk cores. Journal of Petroleum Science and Engineering, 2020, 195: 107654.

Princen, H. M. Capillary phenomena in assemblies of parallel cylinders: I. Capillary rise between two cylinders. Journal of Colloid and Interface Science, 1969a, 30(1): 69-75.

Princen, H. M. Capillary phenomena in assemblies of parallel cylinders: II. Capillary rise in systems with more than two cylinders. Journal of Colloid and Interface Science, 1969b, 30(3): 359-371.

Princen, H. M. Capillary phenomena in assemblies of parallel cylinders: III. Liquid columns between horizontal parallel cylinders. Journal of Colloid and Interface Science, 1970, 34(2): 171-184.

Purcell, W. R. Capillary pressures-their measurement using mercury and the calculation of permeability therefrom. Journal of Petroleum, 1949, 1(2): 39-48.

Skauge, A., Ottesen, B., Vik, B. Variation of special core analysis properties for intermediate wet sandstone material. Paper Presented at the 2003 International Symposium of the Society of Core Analysts (SCA), Pau, France, 22-25

September, 2003.
Skauge, A., Spildo, K., Høiland, L., et al. Theoretical and experimental evidence of different wettability classes. Journal of Petroleum Science and Engineering, 2007, 57(3-4): 321-333.
Skjaeveland, S. M., Siqveland, L. M., Kjosavik, A., et al. Capillary pressure correlation for mixed-wet reservoirs. SPE Reservoir Evaluation and Engineering, 2000, 3(1): 60-67.
Ustohal, P., Stauffer, F., Dracos, T. Measurement and modeling of hydraulic characteristics of unsaturated porous media with mixed-wettability. Journal of Contaminant Hydrology, 1998, 33(1-2): 5-37.
Valvatne, P. H., Blunt, M. J. Predictive pore-scale modeling of two-phase flow in mixed wet media. Water Resources Research, 2004, 40(7): W07406.
Wu, S., Yu, C., Hu, X., et al. Characterization of mineral and pore evolution under $CO_2$-brine-rock interaction at in-situ conditions. Adcances in Geo-Energy Research, 2022, 6(2): 177-178.
Zhao, J., Kang, Q., Yao, J., et al. The effect of wettability heterogeneity on relative permeability of two-phase flow in porous media: A lattice boltzmann study. Water Resources Research, 2018, 54(2): 1295-1311.
Zheng, J., Liu, H., Liu, N., et al. A new pore-scale capillary pressure model for fractional wettability media using cylindrical mixed-wet tubes. International Journal of Multiphase Flow, 2021, 140: 103624.